

Proline 68 Enhances Photoisomerization Yield in Photoactive Yellow Protein

Alisa B. Rupenyan,^{*,†,||} Jocelyne Vreede,[‡] Ivo H. M. van Stokkum,[†] Marijke Hospes,[§] John T. M. Kennis,[†] Klaas J. Hellingwerf,^{†,§} and Marie Louise Groot[†]

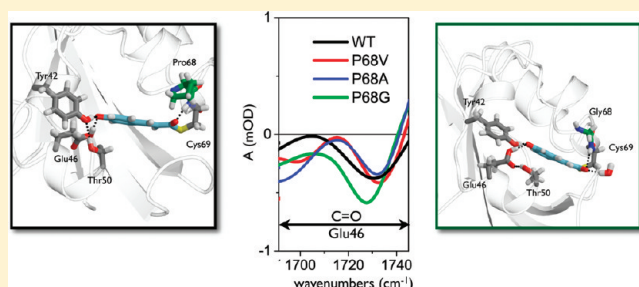
[†]Department of Physics and Astronomy, Faculty of Sciences, Vrije Universiteit, De Boelelaan 1081, 1081 HV Amsterdam, The Netherlands

[‡]Van't Hoff Institute for Molecular Science, University of Amsterdam, Nieuwe Achtergracht 166, 1010 WV Amsterdam, The Netherlands

[§]Laboratory for Microbiology, Swammerdam Institute for Life Sciences, University of Amsterdam, Nieuwe Achtergracht 166, 1010 WV Amsterdam, The Netherlands

 Supporting Information

ABSTRACT: In proteins and enzymes, the local environment of an active cofactor plays an important role in controlling the outcome of a functional reaction. In photoactive yellow protein (PYP), it ensures photoisomerization of the chromophore, a prerequisite for formation of a signaling state. PYP is the prototype of a PAS domain, and the preferred model system for the studies of molecular mechanisms of biological light sensing. We investigated the effect of replacing proline-68, positioned near but not in direct contact with the chromophore, with other neutral amino acids (alanine, glycine, and valine), using ultrafast spectroscopy probing the visible and the mid-IR spectral regions, and molecular simulation to understand the interactions tuning the efficiency of light signaling. Transient absorption measurements indicate that the quantum yield of isomerization in the mutants is lower than the yield observed for the wild type. Subpicosecond mid-IR spectra and molecular dynamics simulations of the four proteins reveal that the hydrogen bond interactions around the chromophore and the access of water molecules in the active site of the protein determine the efficiency of photoisomerization. The mutants provide additional hydrogen bonds to the chromophore, directly and by allowing more water molecules access to its binding pocket. We conclude that proline-68 in the wild type protein optimizes the yield of photochemistry by maintaining a weak hydrogen bond with the chromophore, at the same time restraining the entrance of water molecules close to the alkylic part of pCa. This study provides a molecular basis for the structural optimization of biological light sensing.



INTRODUCTION

Photoactive yellow protein (PYP) is a bacterial photoreceptor from *Halorhodospira halophila*.¹ Upon absorption of blue light, its chromophore, *p*-coumaric acid (pCa), undergoes *trans*–*cis* isomerization around its C=C bond, marking the beginning of a photocycle and the formation of a signaling state that involves partial unfolding of the protein.² The protein tunes the absorption spectrum of the pCa chromophore from 284 nm, in solution, to 446 nm, and provides an optimal environment for its photochemistry. Gas phase spectroscopy studies show that the absorption maximum of pCa in the protein is very similar to that of the isolated chromophore in the gas phase, apparently suggesting that the protein provides a vacuum-like environment for the chromophore.³ On the other hand, there are several studies in which replacement of residues near the chromophore results in major spectroscopic shifts; see, for example, Philip et al. (ref 4), showing there is significant interaction of the chromophore with its protein surrounding. A recent computational study⁵ of the

tuning effect of the protein on the absorption of pCa demonstrates that the small shift between chromophore absorption in vacuum and within the protein is due to the balance between two opposing effects, i.e., the change of the structure of the chromophore inside the protein and perturbations from the protein environment on the excitation energy.

If pCa is in solution or in the denatured protein, it photoionizes or forms twisted *trans* conformations, that relax back to the *trans* ground state,^{6–8} but it does not form stable photo-products. Bound to the PYP protein, pCa isomerizes from the *trans* to *cis* conformation with a quantum yield of about 0.35.^{2,9–12} In the dark, the protein keeps pCa in a fixed conformation (Figure 1), via a covalent thioester bond to residue Cys69 and hydrogen bonds to surrounding residues.^{13,14} The oxygen in the

Received: December 21, 2010

Revised: March 24, 2011

Published: May 04, 2011

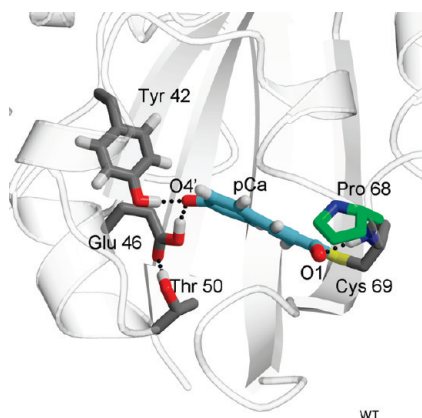


Figure 1. The chromophore-binding pocket of wt PYP. Para-coumaric acid (pCa) and the neighboring hydrogen-bonded residues are represented as sticks. The phenolate oxygen atom is labeled as O4' and the carbonyl oxygen as O1. Proline 68 is indicated in green color. The phenolate ring of pCa is restrained by a hydrogen bond network including residues Glu46 and Tyr42, and indirectly Thr50 and Arg52 (not shown).

carbonyl group of pCa ($O1_{pCa}$) forms a hydrogen bond to the backbone nitrogen atom of Cys69.¹⁵ During the photoisomerization process, this bond is broken and the carbonyl flips relative to the plane of the aromatic ring, resulting in C=C *trans*–*cis* isomerization and subsequent entry into the photocycle.^{9,10,15,16} In unsuccessful isomerization attempts, the chromophore assumes a distorted conformation with this hydrogen bond still intact, suggesting that the strength of this bond controls the quantum yield of the photocycle.⁹

PYP is attractive for studying how the interaction between protein backbone, amino acid side chains, water molecules, and cofactor results in activity, which in the case of PYP consists of the storage of photon energy and the generation of a biological signal. Due to its size, pCa is one of the simplest chromophores found in photoreceptors, with only one isomerizable double bond. Several structures of photocycle intermediates are available.^{11,17–19} Here, we investigate the effect of a single residue, proline 68, on the functionality of PYP. Pro68 does not bind to pCa directly but neighbors the covalent linker Cys69 and is positioned as a lid of the chromophore-binding pocket. A concerted motion of Pro68, Tyr98, and the thioester linkage of the chromophore has been suggested to facilitate the C=O flip during isomerization.¹⁴ Residues smaller than proline may result in a weaker hydrogen bond between the C=O of pCa and the backbone, lowering the energy required to break this bond and thereby facilitate isomerization⁹ and thus increase the quantum yield of photoactivation. However, because proline is an imino acid in which the backbone cannot act as a hydrogen bond donor, mutating it will provide an additional hydrogen bond donor and will change the local flexibility in the vicinity of the chromophore.

We identify the factors that determine the isomerization quantum yield through the application of ultrafast spectroscopy and molecular dynamics simulations. The isomerization yield is significantly lower in the P68V, P68A, and P68G mutants, with a larger effect for the smaller residues. Molecular dynamics (MD) simulations of the WT and mutant proteins reveal that several structural and dynamical differences correlate with the progressively lower quantum yield observed for the smaller amino acids. Recordings of the hydrogen bond strength involving the pCa

carbonyl group, through time-resolved mid-infrared spectroscopy, corroborate the MD simulations. We show that proline 68 is effective in limiting the water access to the chromophore and in optimizing the hydrogen bond interactions between the chromophore and its environment.

MATERIALS AND METHODS

Visible Light Spectroscopy in the Subpicosecond to Nanosecond Time Range. The experimental setup consists of an integrated Ti:sapphire oscillator-regenerative amplifier laser system (Coherent Legend-UHP) operating at 1 kHz and at a central wavelength of 800 nm, producing 85 fs pulses of 2.5 mJ. Part of this 800 nm light is frequency doubled in a BBO crystal to generate the 400 nm excitation (pump) pulses. A second portion of the 800 nm light is focused into a laterally rotating CaF_2 plate to generate white light for the probe. After overlap in the sample, the probe is dispersed by a 15 cm focal length spectrograph (Oriol) onto a home-built photodiode array detector. The polarization of the pump is set to the magic angle (54.7°) with respect to the probe pulse. A phase-locked chopper on the pump beam pathway, operating at 500 Hz, ensures that an absorbance difference spectrum can be calculated. To ensure a fresh spot on the sample for each laser shot, the sample is moved by a home-built Lissajous scanner. The energy of the excitation pulse is 200 nJ. The instrument response function is ~ 150 fs. The pump beam excites 5% of the present proteins in the probed volume.

Ultrafast mid-IR Spectroscopy. The experimental setup (see ref 15 for a more detailed description) consists of an integrated Ti:sapphire oscillator/regenerative amplifier (Hurricane; SpectraPhysics, Mountain View, CA) operating at 1 kHz and producing 0.8 mJ pulses of 80 fs. The output of this laser is used to pump a commercial optical parametric amplifier (TOPAS; Light Conversion, Vilnius, Lithuania), resulting in a broad infrared pulse with a spectral width of $\approx 200\text{ cm}^{-1}$. A home-built HgCdT camera system placed behind a spectrograph is read out every shot at a repetition rate of 1 kHz and a sampling resolution of $\approx 6\text{ cm}^{-1}$. Another part of the Hurricane output is used to pump a home-built noncollinear optical parametric amplifier to generate pulses at 475 nm with duration of ≈ 60 fs and 200 nJ excitation energy. The instrument response function is ≈ 200 fs (cross-correlation in GaAs). The setup is contained in a nitrogen-purged box to reduce distortions of the IR beam by water vapor absorption. The transient absorption spectra resulting from the pump–probe measurement are shown in Figure 2.

Global Analysis. For each mutant, all 80 time-gated spectra (measured at 256 wavelengths) were collated in a matrix, which was globally fitted using a sequential kinetic scheme with increasing lifetimes.²⁰ From this matrix, the lifetimes and the evolution-associated difference spectra (EADS) were estimated. The quality of the fit was judged by inspection of the first two pairs of singular vectors of the matrix of residuals, which had to be structureless. The instrument response function was described by a Gaussian, and the white-light dispersion over the spectral range was modeled as a second-order polynomial. With increasing lifetimes, and thus decreasing rates, the first of the EADS decays with the first lifetime and corresponds to the difference spectrum at time zero with an ideal, infinitely small instrument response function. The second of the EADS is formed with the first lifetime and decays with the second lifetime. The fifth of the EADS (the final one) represents the difference spectrum of the longest-living species. The error in the lifetimes obtained from

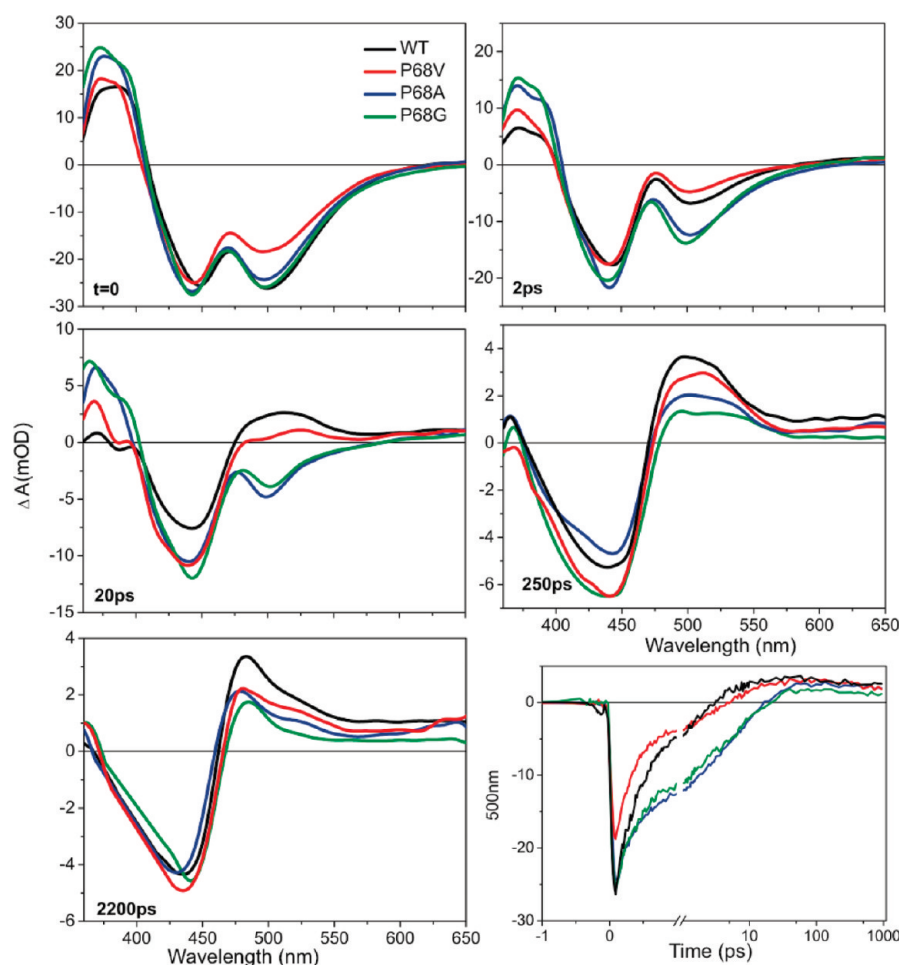


Figure 2. Transient absorption data of wt PYP and mutants. Top panel: Difference absorption spectra recorded at specific time delays. The bottom right panel shows time traces recorded at $\lambda = 500$ nm for the PYP mutants and the wt.

the fitting procedure does not exceed 10%. In general, EADS represent a mixture of species, and they are interpreted as a weighted sum (with only positive contributions) of species-associated difference spectra (SADS).

Target Analysis. To resolve the SADS from EADS, a kinetic scheme, shown in Figure 3 (upper panel), is used. Because of the strongly overlapping contributions of the different intermediates, more than one set of parameters can produce a satisfactory fit. Continuous comparison of the SADS and the concentration profile for each species with the time-dependent evolution of the absorption (Figures 2 and 3, middle panel) and spectra derived from sequential analysis (Supporting Information, Figure S1) is crucial for determining the most physically plausible set of parameters. The concentration profiles in Figure 3 follow closely the absorption changes shown in Figure 2, and the set of four corresponding spectra is physically realistic; i.e., the bleached ground state absorption band is similar in magnitude in each SADS, and each SADS has features in accordance with the raw data and with its nature: for the excited state (ES), the corresponding signatures are the stimulated emission and excited state absorption, for the following (red) SADS the induced absorption band around 470 nm and the last two SADS (blue and green) are characterized by the induced absorptions at wavelengths >500 nm.

Selected time traces together with the fit resulting from the application of the model depicted in Figure 2 are shown on

Figure S2 of the Supporting Information. As this analysis implements the condition to yield only one set of spectra for all samples, the fit of the data can be improved by removing this condition. We performed the analysis using the same model but releasing the constraint of equality of the spectra. The rate constants, the branching ratios, and the quantum yields of all samples remain qualitatively the same, but the fit is improved, as small differences in the absorption of the samples are taken into account. The four sets of SADS resulting from simultaneous analysis of the four data sets are shown in Figure S3A of the Supporting Information, and the time traces together with the fit are shown in Figure S3B.

All parameters derived from target analysis are summarized in Tables S1 and S2 of the Supporting Information. The initial populations and the rate constants of the transitions are shown in Table S1, and the lifetimes of the species are shown in Table S2.

Molecular Dynamics—Force Field Simulation. The molecular dynamics simulations were performed using GROMACS, version 4.0.4,²¹ using the AMBER-03 force field²² with TIP3P water.²³ The starting conformations for wt PYP were obtained from the atomic resolution crystal structure of the dark state (PDB code 1NWZ (ref 14)), and for the mutants, Pro68 was altered into valine, alanine, and glycine using Modeler (version 8.2).²⁴ The structures were placed in a periodic dodecahedron box, filled with TIP3P water²¹ after adding hydrogen atoms to all

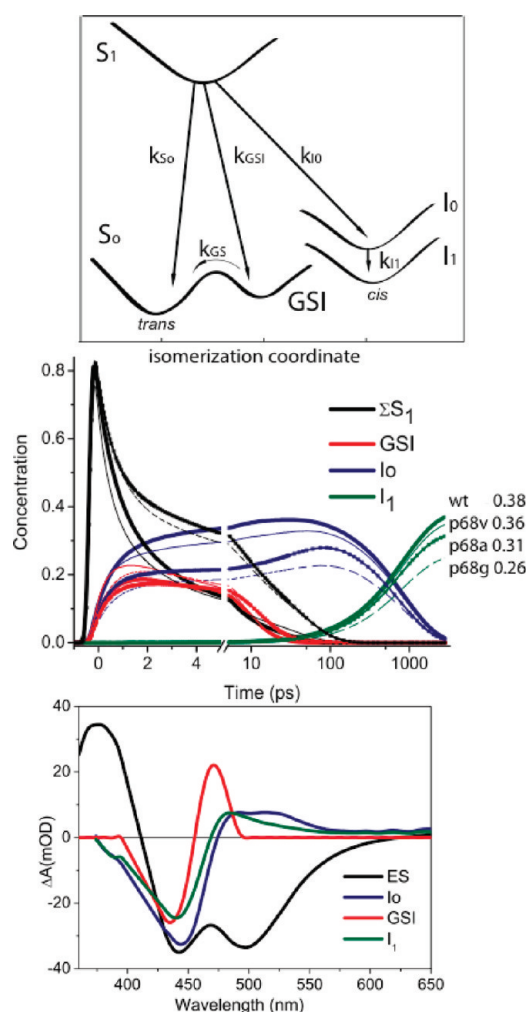


Figure 3. Target analysis of the transient absorption data. Upper panel: Schematic representation of the target model used for the analysis. The three initial excited states (ES1, ES2, and ES3) are represented by the S1 potential energy surface. The rates connecting each state (Supporting Information, Table S2) are allowed to vary between the samples, but the species-associated difference spectra of each state are assumed to be identical for all samples. The isomerization coordinate is a single, condensed, reaction coordinate that includes, at least, rotation around dihedral angles and hydrogen bond breaking. The exact conformation of the chromophore in the GSI state remains to be determined. Middle panel: Concentration profiles of each state, for all four PYP proteins, as derived from the data. The quantum yield of the final photoproduct I_1 (green lines) is indicated for every protein. The concentration profiles of ES1, ES2, and ES3 (black) are summed up for better readability. The time scale is linear up to 5 ps and logarithmic from 5 ps to 3 ns. Bottom panel: Species associated difference spectra (SADS) resulting from the target analysis. The spectra are color-coded to match the states from the middle panel.

conformations. Water molecules overlapping with the protein were removed, as well as waters not hydrogen bonding to the bulk. The system charge was neutralized by adding 150 mmol/L of NaCl (WT: 16 Na^+ , 10 Cl^- ; P68V: 16 Na^+ , 10 Cl^- ; P68A: 15 Na^+ , 9 Cl^- ; P68G: 16 Na^+ , 10 Cl^-). The resulting systems were then energy minimized using the conjugate gradient method. Then, the positions and velocities of the hydrogen atoms and water molecules were equilibrated for 10 ps at 300 K and 1 bar, while the protein heavy atoms were position restrained. After

release of the restraints on the protein atoms, the systems were equilibrated for 50 ns, followed by 55 ns of sampling, saving coordinates every 2 ps. The temperature was kept constant at 300 K using the velocity-rescaling thermostat,²⁵ while pressure remained constant at 1 bar with the use of the Parrinello–Rahman barostat.²⁶ Nonbonded interactions were treated with a cutoff at 1.1 nm, while long-range electrostatics were treated with PME.^{27,28} All bonds were constrained using the LINCS algorithm²⁹ and SETTLE for water,³⁰ allowing for a time step of 2 fs. From the resulting trajectories, we calculated several distances and the number of water molecules around a residue using a combination of GROMACS tools and perl scripts. The simulations were performed on the Dutch National Compute Cluster LISA.

Protein Purification. Site-directed mutagenesis was performed using the QuickChange kit (Stratagene) and confirmed by DNA sequencing.³¹ Wild type PYP and its P68A, P68G, and P68V mutant derivatives were expressed and isolated as described previously for wild type PYP.³² The samples were concentrated and placed between two CaF_2 windows, separated by a 50 μm Teflon spacer, at $\text{OD}_{446} \approx 0.6$.

RESULTS

Transient Absorption Difference Spectra in the 360–650 nm Region. The absorption of the pG state (ground state) is peaking at 446 nm for PYP WT and P68A, at 445 nm for P68V, and at 444 nm for P68G (Supporting Information, Figure S4).

In WT, I_0 forms in a few picoseconds and is characterized by a broad red-shifted absorption in the region 460–500 nm. The second *cis* intermediate, I_1 (or pR, PYP_L), forms in 1–3 ns and absorbs maximally at 475 nm.^{33–35}

The time-dependent absorption changes at selected time points, induced by excitation at 400 nm with a ~ 100 fs laser pulse, are shown in Figure 2. The first snapshot, at $t = 0$, is dominated by the excited state absorption of pCa at 370 nm, and furthermore exhibits the negative contribution of the ground state at 446 nm, and of stimulated emission (SE) at 500 nm. The spectra at $t = 0$ are similar for all samples, apart from a reduction in SE in P68V, and increased excited state absorption (ESA) in P68A and P68G. In the 20 ps snapshot, the spectra of WT and P68V are positive around 500 nm, indicating formation of I_0 , whereas for P68A and P68G the SE contribution persists, indicating slower decay of the electronically excited state of pG and build-up of I_0 . The snapshots at 250 and 2200 ps show similar positive absorption bands for all samples resembling the absorption of the product states I_0 and I_1 , respectively.^{33–36} Clearly, the mutants have lower yield of I_1 formation, as indicated by the height of the absorption at 480 nm. The excited state (ES) absorption decay is multiexponential, and three exponential decay times, on the order of hundreds of femtoseconds, picoseconds, and tens of picoseconds, respectively, have to be introduced to fit the kinetic traces, plus a component of 830 ps describing the I_0 to I_1 transition. The decay times are different for the four samples, reflecting faster ES decay and product formation for WT and P68V (Figure 2; see Figure S1 in Supporting Information for the evolution associated difference spectra). It has been shown, for proteins that exhibit a multiexponential excited state decay, that the faster excited state decay is correlated to the higher product yield branch of the photoreaction, whereas the fraction of molecules that decay slowly are more likely

to decay directly to the ground state, or to the ground state intermediate.^{33,37}

Estimation of the Quantum Yield of Photoisomerization for PYP wt, P68V, P68A, and P68G. To quantify the observation of the lower I_1 quantum yield in the mutants, and the difference in decay kinetics, we applied target analysis. In this analysis, the data from all four samples are fitted simultaneously to a model (Figure 3) consisting of three excited states (S_1) to account for the multiexponential decay of the excited state (probably arising from heterogeneity of the sample¹¹), the I_0 and I_1 product states, a ground state intermediate (GSI), and the ground state (GS). The initial population of each excited state (Supporting Information, Table S1) is estimated from the relative amplitudes of the contributions of the three rates (an indication for the contribution of each excited state is the area of the corresponding stimulated emission band, estimated from the EADS, Supporting Information, Figure S1). The excited-state SADS (black, Figure 3) is characterized by a positive excited state absorption (360–410 nm), ground state bleach (410–460 nm), and stimulated emission band (460–610 nm). The SADS of the ground state intermediate (red) has a positive absorption band peaking at 470 nm. The positive absorption in the SADS of the product state I_0 (blue) is peaking at 530 nm. The positive absorption band of the SADS of the final state I_1 (green) is blue-shifted and narrowed compared to I_0 . The reduced amplitude of the ground state bleach in I_1 compared to I_0 can be explained by the increased overlapping of the absorption of the blue-shifted I_1 with the ground state bleach, although losses due to molecules decaying from I_0 to the ground state cannot be completely excluded.

The GSI is a short-lived spectroscopic intermediate that decays to the ground state and represents unsuccessful attempts of the protein to enter the photocycle.^{9,33,38} For simplification, its lifetime is set identically for all samples. The transition from state I_0 to I_1 is set to occur with a 100% yield, following Van Wilderen et al. (ref 9). In the simultaneous target analysis, each data set (i.e., wt, P68A, P68V, P68G) is scaled over the full wavelength range with a parameter to correct for small amplitude differences, caused by differences in sample concentration or optical alignment.

The spectral shapes for the species associated difference spectra (SADS) and the corresponding lifetimes (Figure 3) derived from the target analysis are consistent with those observed in previous time-resolved absorption and fluorescence studies on WT PYP.^{33,35,38–40} A set of time traces with corresponding fits is shown in Figure S2 of the Supporting Information. We further performed target analysis using the same model but releasing the constraint of equality of the spectra. The rate constants, the branching ratios, and the quantum yields of all samples remain the same, but the fit is improved, as small differences in the intensity of the excited state absorption and stimulated emission, relative to the ground state bleach signal, are allowed for. These differences may be a direct consequence of the altered interactions of the pCa chromophore with its environment, as a result of the mutations. The four sets of SADS, resulting from this simultaneous analysis of the four data sets, are shown in Figure S3A (Supporting Information), and the time traces together with the fit are shown in Figure S3B (Supporting Information).

The applied model, with the severe constraint of using the exact same set of four spectra for each mutant, results in a good fit of all data sets. Therefore, it allows us to quantify the dynamics of

Table 1. Quantum Yields of Photocycle Intermediates, Derived from Target Analysis^a

	I_0	GSI	GS
WT	0.38	0.30	0.32
P68V	0.36	0.33	0.31
P68A	0.31	0.47	0.22
P68G	0.26	0.48	0.26

^a The relative error in all yields is ± 0.01 .

photoisomerization for each mutant and to determine the role of proline 68 in the reaction. The quantum yield of photoisomerization is highest for WT, and gradually decreasing for P68V, P68A, and P68G, from 0.38 to 0.26 (Table 1). The current approach, in which the different samples are compared in a consistent experimental and analytical approach, ensures that the relative error in the determined quantum yield is significantly smaller than the absolute error, and we estimate it to be less than 0.01. Previously, the overall photocycle yield of the P68A mutation has been estimated to be similar to the wt yield⁴¹ (based on the yield of the pB state), or even slightly higher,⁴² although the fluorescence yield of the mutant has been shown to be enhanced,⁴³ and its excited state decay is slower.

Molecular Dynamics Simulations of the P68V, P68A, and P68G Mutants and wt PYP. PYP is an excellent model system to study the factors that are used in a protein to tune the photochemistry of its chromophore to a reaction outcome very different from that in solution. To investigate the structural effects of the mutations on the environment of pCa, we performed force field molecular dynamics (MD) simulations (105 ns runs for each protein system) and transient mid-infrared spectroscopy. We note that, since these are ground state simulations, they are not sensitive to the excited state dynamics and to the structural changes induced by the photoreaction, but they provide structural information before photoexcitation of pCa. The absorption changes following photoexcitation have been recently accessed by QM/MM and *ab initio* computational methods.^{44,45} As shown by gas-phase experiments³ and recent QM/MM calculations,^{5,44} the absorption of the chromophore is finely tuned precisely by the protein environment and the residues in the vicinity of pCa.

The UV/vis spectra indicate little difference in the electrostatics of the chromophore-binding pocket, when comparing the proline-68 mutants to wt; therefore, the simulations should reproduce similar interactions around pCa. In wt, Tyr42 and Glu46 act as hydrogen bond donors to the phenolic oxygen O4' of pCa. At the start of the simulations of all four systems, the hydrogen bond between Glu46 and pCa is absent but reforms after at most 40 ns (for the valine mutant), and then remains intact; see inset of Figure 4a. Therefore, we used the data starting from 50 ns for our analyses, which include the distances between atoms participating in hydrogen bonds between the chromophore and the protein. For all four systems, the phenolic oxygen O4' forms hydrogen bonds with Glu46 (Figure 4a) and Tyr42 (Figure 4b). Then, we monitored how the strength of the hydrogen bond between O1_{pCa} and Cys69 is affected by the mutations.

All simulations sampled a distance of 0.2 nm between O1_{pCa} and the backbone nitrogen N of Cys 69 most of the time. This distance indicates that a hydrogen bond is formed between these atoms.

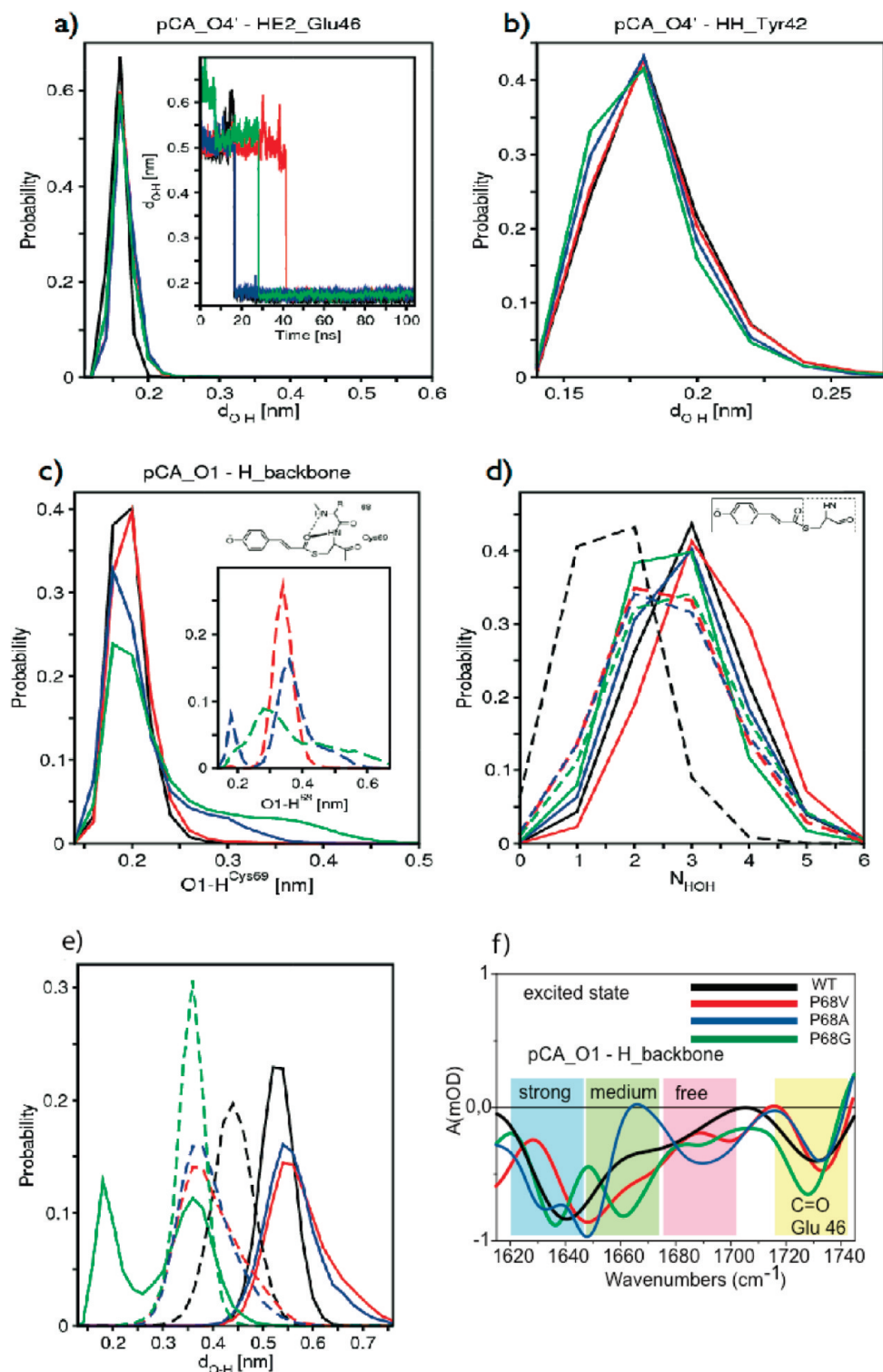


Figure 4. Hydrogen bonds in the chromophore-binding pocket. (a) Distribution of the distance between phenolate oxygen atom O4' in pCa and hydrogen atom HE2 in Glu46. The bin size is 0.02 nm. The inset shows this distance as a function of the simulation time. (b) Distribution of the distance between phenolate oxygen atom O4' in pCa and hydrogen atom HH in Tyr42. The bin size is 0.01 nm. (c) Distribution of the distances between thioester oxygen atom O1 in pCa and backbone hydrogen atoms H in Cys69 (solid lines) and residue 68 (dashed lines, in inset). Note that Pro68 in wt PYP cannot act as a hydrogen donor. The bin size is 0.02 nm. (d) Number of water molecules within a radius of 0.35 nm of pCa (solid lines) and of Cys69 (dashed lines). The bin size is 1. (e) Distribution of the distance between oxygen atoms OE1 (solid lines) and OE2 (dashed lines) in the side chain of Glu46 and the hydrogen atom HG1 in Thr50. The bin size is 0.01 nm. (f) Mid-IR absorption difference spectra of the wt, P68V, P68A, and P68G excited states, as obtained from a global analysis on data sets consisting of 32 wavelengths and 65 time points. The negative signals correspond to the vibrational frequency of the pCa carbonyl in the ground state of the chromophore (1630–1660 cm⁻¹), and of the carbonyl of Glu46 (1720–1740 cm⁻¹).

The mutants have an additional hydrogen bond donor in their backbone close to the carbonyl end of pCa. We monitored the distance between the backbone hydrogen atom of residue 68 and the carbonyl oxygen O1 of the chromophore, displayed in the inset of Figure 4C. For P68A, there is an additional hydrogen bond between the chromophore and the protein backbone, evidenced by the peak at 0.2 nm. This hydrogen bond also appears in the valine mutant for a limited time, as well as an additional conformation at $d_{\text{O1-H}} = 0.36$ nm, which represents a water-mediated hydrogen bond between the backbone of Val68 and pCa. The glycine mutant samples a broad range of configurations, including the double hydrogen bond, the water mediated hydrogen bond, and no interaction at all. The broader distribution for the backbone-chromophore distances indicates that the backbone of Gly68 and Cys69 exhibits more flexibility in comparison to the three other systems.

Figure 4d shows the number of water molecules within 0.35 nm of pCa (solid lines) and Cys69 (dashed lines). For the water content around pCa, the mutation has little effect, whereas the mutants have more water molecules around the protein backbone, in comparison to proline (i.e., wt). This means that, although the mutation increases the hydrophilicity around the carbonyl end of pCa, the water molecules do not enter further into the protein core.

Nevertheless, the mutation of Pro68 to glycine has a significant effect on the hydrogen bond network at the phenolic oxygen end of the chromophore. In the wild type, the negative charge on the side of pCa is stabilized by hydrogen bonds to Tyr42 and Glu46, and via Tyr42 to Thr50. In our simulation(s), Thr50 fluctuates between interacting with the side chain of Tyr42 and the backbone atoms of Glu46. In the simulations of the mutants, Thr50 participates directly in the hydrogen bond network of pCa. For wt, P68V, and P68A, oxygen OE1 of Glu46 does not form any hydrogen bonds, as shown by the solid lines in Figure 4e peaking at 0.55 nm. In the glycine mutant, this atom does have a hydrogen bond interaction, with Thr50.

Transient Absorption Difference Spectra in the mid-IR. We monitored the spectral region of the carbonyl ($\text{C}=\text{O}$) stretch vibrations involved in the hydrogen bond network using time-resolved spectroscopy, since these bands would be hidden by absorption from the protein in a steady-state absorption experiment (Figure 4f). We performed global analysis using a sequential model, and the spectra corresponding to a rate constant of a few tens of picoseconds are shown in Figure 4f. They are dominated by the negative contribution of bleached absorption from the vibrations of PYP in the ground state,^{9,15} allowing us to assess the hydrogen bond interactions of the carbonyl groups prior to photon absorption. The $\text{C}=\text{O}$ stretch of pCa is positioned at ~ 1640 cm^{-1} and progressively up-shifts when the hydrogen bond to Cys69 weakens, or is absent.^{9,46} In the IR spectra, we observe that the predominant bands for WT and P68V are positioned at ~ 1640 and ~ 1650 cm^{-1} , respectively, and the up-shifted bands, peaking in the region 1660–1690 cm^{-1} , are weaker. P68A and P68G show a band peaking at 1630–1635 cm^{-1} , indicating a stronger hydrogen bond to the pCa carbonyl than in WT. However, there are also two more bands at higher frequency, indicating multiple conformations in which the hydrogen bond between O1_{pCa} and Cys69 is perturbed. The $\text{C}=\text{O}$ stretch of Glu46 is positioned at 1730–1740 cm^{-1} ^{9,15,46} and down-shifts upon stronger hydrogen bond interactions of Glu46. We observe a shift in this vibration for the glycine mutant.

DISCUSSION

Our results show that replacing proline 68 in PYP, with either larger or smaller neutral amino acids, leads to a reduction in the isomerization yield. The population of the GSI is higher for the mutants showing lower isomerization yield, suggesting that pCa attempts to enter the photocycle, distorting from the *trans* conformation, but is unable to successfully complete the flip of the carbonyl. As a result, pCa falls back to the GSI state more often in the mutants than in WT (see Table 1, Figure 1, and Figure 3). The spectral shifts introduced by the mutations are within 1 nm, suggesting that the effect on the charge distribution around the chromophore is considerably small. Therefore, the decrease in the yield, introduced by the mutations, is mainly due to sterical effects, rather than alterations of the charge distribution around the chromophore. As the residue at position 68 is not directly in contact with the chromophore, mutating it allows for the estimation of the collective effects introduced by rearrangements in the chromophore-binding pocket, and in the protein backbone. The observations from the MD simulations correlate well with the hydrogen bond interactions deduced from positions of the ground state bleaches observed in the mid-infrared absorption difference spectra of PYP, recorded on a picosecond time scale. Furthermore, the trend in the population of the hydrogen bonded state between O1_{pCa} and N of Cys69 follows the trend in quantum yield decrease.

We can now summarize the structural effects in the chromophore-binding pocket, induced by mutation of proline 68:

- (i) Replacement with smaller residues strengthens the interaction between chromophore and protein by facilitating an additional hydrogen bond to pCa. This additional hydrogen bond shortens the distance of the hydrogen bond between pCa and Cys69. Breaking of the hydrogen bond between chromophore and protein backbone has been shown in earlier QM/MM simulations to be a key event during isomerization,⁴⁷ and the strength of this interaction was suggested to control the quantum yield of the photocycle.^{9,11} The IR spectra show three bands for the alanine mutant, in particular one at 1630 cm^{-1} , indicating a stronger hydrogen bond interaction for the pCa carbonyl oxygen atom, compared to wild type. A similar band is present in the spectra of the glycine mutant, peaking at 1635 cm^{-1} . During the simulation of the P68A system, the hydrogen bond pattern around the carbonyl oxygen fluctuated, exhibiting one or two hydrogen bond interactions to the protein backbone but also no such interactions at all (cf bands in the IR spectra at 1648, 1630, and 1690 cm^{-1}). The fluctuating distance between O1_{pCa} and the nitrogen of residue 68 indicates that the backbone of the alanine and glycine mutants is more flexible.
- (ii) Replacement with a bulkier residue (valine) provides an additional water-mediated hydrogen bond with the protein backbone that corresponds to the up-shifted band peaking at 1645 cm^{-1} in the IR spectrum. The alanine mutant has a similar band, possibly indicating that this mutant also forms water-mediated interactions. The weaker water-mediated interaction does not have a big effect on the quantum yield, evidenced by the modest decrease of 0.02 for P68V.
- (iii) Replacement with a small and flexible residue (glycine) can also result in a complete disruption of the hydrogen bond interactions with the protein backbone. This

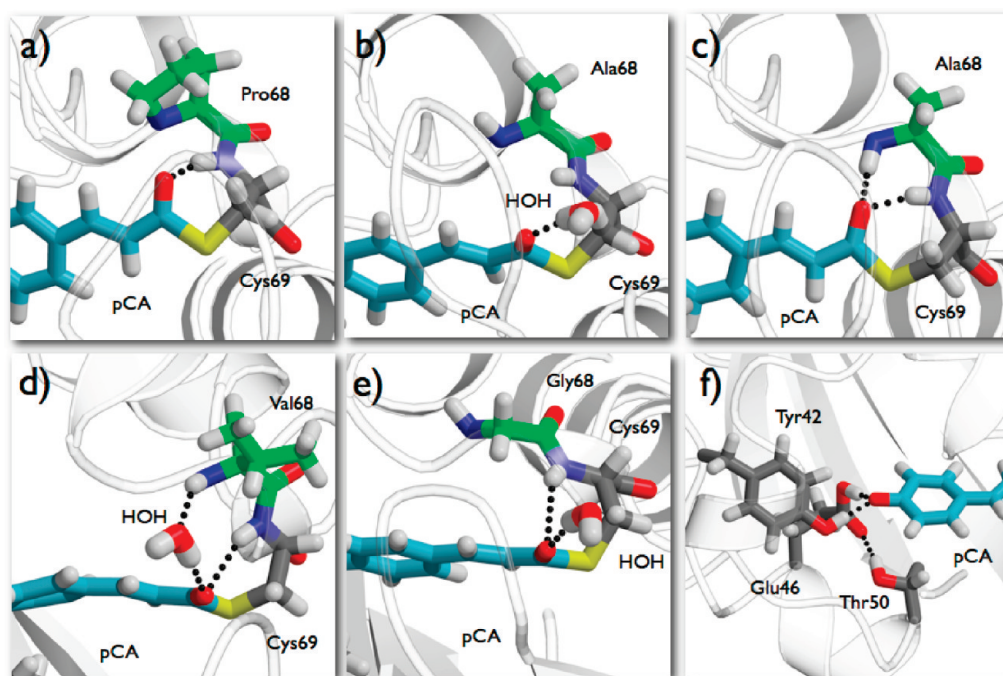


Figure 5. Snapshots of the hydrogen bond patterns of pCa in the mutants. (a,b) Single hydrogen bond to the protein backbone for WT (a) and P68A (b). (c) Double hydrogen bond to the protein backbone. (d) One direct and one water-mediated hydrogen bond to the protein backbone. (e) Hydrogen bond to water. (f) Altered interaction of Glu46 with the chromophore-binding pocket. Visualization is as described in Figure 1. The residues at position 68 are shown in green, pCa is shown in light-blue, and residues in the hydrogen bonding network in gray color.

“unbound” state is reflected in the data by the band peaking at 1665 cm^{-1} . The simulation of the glycine mutant showed that the carbonyl oxygen could have one or two hydrogen bond interactions with the protein backbone but also none at all (cf bands in the IR spectra at 1660, 1635, and 1690 cm^{-1}).

- (iv) All mutations induce rearrangements in the hydrogen bond network around the phenolic part of pCa. This is clearly observable in the vibrational spectra of the P68G mutant, where the C=O stretch vibration of Glu46, which is similar to wild type for P68A and P68V, shows a down-shift, indicating that the carbonyl oxygen of Glu46 is involved in hydrogen bonding. Our simulation of the glycine mutant indicates that Glu46 indeed forms a hydrogen bond with Thr50.

These hydrogen bond rearrangements possibly influence the formation of the signaling state and the ground state recovery. The protonation of the phenolic oxygen atom of pCa preceding the conformational change in the pB state might occur via a different pathway.

Although there is experimental evidence that the proton donor in the pB state is Glu46,⁴⁸ it cannot be excluded that water molecules can also donate a proton via the hydrogen bond network. It has been suggested by computational studies that water coordination to Glu 46 plays an important role for the stabilization of the proton transfer reaction.⁴⁹ Considering the facilitated access of water molecules, and the rearrangement around the phenolic moiety of pCa in the chromophore-binding pocket, especially for P68A and P68G this mechanism is to be considered. Although the mutation introduced at position 68 does not dramatically change the photocycle recovery rates measured at longer time scales (Supporting Information, Table

S3), the trend is in agreement with the observations made in the picosecond–nanosecond transient absorption measurements, and the recovery of the glycine mutant is the slowest.

CONCLUSIONS

We have investigated the role of a single amino acid in the photocycle of PYP. We replaced proline-68, positioned near but not in direct contact with the chromophore, with other neutral amino acids (alanine, glycine, and valine), and used ultrafast spectroscopy probing the visible and mid-IR spectral regions, and molecular simulation to understand the modified interactions, tuning the efficiency of light signaling. We find that the quantum yield of photoisomerization of pCa in PYP is highest for the wt protein. Our vibrational difference spectra indicate that, for the four proteins studied, the hydrogen bonding network around pCa in the ground state is different, and we access these differences in detail by applying MD simulations for wt, P68V, P68A, and P68G. Combining the observations from the MD simulations and the IR measurements, we can identify four different hydrogen bond patterns around the carbonyl oxygen O1 of pCa, shown in Figure 5. These four states are the single hydrogen bond (Figure 5a), the single hydrogen bond with additional water (Figure 5b), the double hydrogen bond (Figure 5c), the single hydrogen bond with an additional water-mediated hydrogen bond to the protein backbone (Figure 5d), and no hydrogen bond (Figure 5f). The hydrogen bond network around the phenolic part of P68G is shown in Figure 5e. The consistency between simulations and experimental data provides detailed insight of the molecular machinery involved in biological signal transduction.

This study confirms experimentally that hydrogen bonding interactions around the chromophore are critical for the optimal

photosensing of PYP,⁵⁰ and indeed, to our knowledge, so far there has been no mutation around pCa that can increase the efficiency of light sensing. Such a mutation (or a combination of mutations) would require maintaining a similar or a weaker hydrogen bond between O1_{pCa} and the backbone hydrogen of Cys69, and at the same time restraining the entrance of water molecules close to the alkylic part of pCa. A good candidate to start with is phenylalanine, at position 68, as it is bulky enough to maintain the rigidity of the protein backbone in the vicinity of pCa, and hydrophobic enough to maintain the water molecules from entry in the chromophore binding pocket.

■ ASSOCIATED CONTENT

S Supporting Information. Figures showing EADS, time traces, SADS, and absorption spectra and tables showing additional data. This material is available free of charge via the Internet at <http://pubs.acs.org>.

■ AUTHOR INFORMATION

Corresponding Author

*E-mail: a.b.rupenyan@uva.nl

Present Addresses

^{||}Laboratorium für physikalische Chemie, ETH Zurich, Wolfgang-Pauli-Strasse 10, 8093 Zurich, Switzerland.

■ ACKNOWLEDGMENT

This research was supported by The Netherlands Organization for Scientific Research and the Human Frontier Science Program. J.V. thanks Gerrit Groenhof at the Max Planck Institute for Biophysical Chemistry, Goettingen, Germany, for kindly providing the force field parameters of the chromophore. A.B.R. thanks Jos Thieme from VU University Amsterdam for technical support.

■ REFERENCES

- (1) Meyer, T. E.; Tollin, G.; Hazzard, J. H.; Cusanovich, M. A. Photoactive yellow protein from the purple phototrophic bacterium, *E. halophila*: Quantum yield of photobleaching and effects of temperature, alcohols, glycerol, and sucrose on kinetics of photobleaching and recovery. *Biophys. J.* **1989**, *56*, 559–564.
- (2) Genick, U. K.; Soltis, S. M.; Kuhn, P.; Canestrelli, I. L.; Getzoff, E. D. Structure at 0.85 Å resolution of an early protein photocycle intermediate. *Nature* **1998**, *392*, 206–209.
- (3) Nielsen, I. B.; Boyé-Pérone, S.; El Ghazaly, M. O. A.; Kristensen, M. B.; Brøndsted Nielsen, S.; Andersen, L. H. Absorption spectra of photoactive yellow protein chromophores in vacuum. *Biophys. J.* **2005**, *89*, 2597–2260.
- (4) Philip, A. F.; Eisenman, K. T.; Papadantonakis, G. A.; Hoff, W. D. Functional tuning of photoactive yellow protein by active site residue 46. *Biochemistry* **2008**, *47*, 13800–13810.
- (5) Rocha-Rinza, T.; Sneskov, K.; Christiansen, O.; Ryde, U.; Kongsted, J. Unraveling the similarity of the photoabsorption of deprotonated p-coumaric acid in the gas phase and within the photoactive yellow protein. *Phys. Chem. Chem. Phys.* **2011**, *13*, 1585–1589.
- (6) Larsen, D. S.; Vengris, M.; van Stokkum, I. H. M.; van der Horst, M.; de Weerd, F. L.; Hellingwerf, K. J.; van Grondelle, R. Photoisomerization and photoionization of the photoactive yellow protein chromophore in solution. *Biophys. J.* **2004**, *86*, 2538–2550.
- (7) Mataga, N.; Chosrowjan, H.; Shibata, Y.; Imamoto, Y.; Kataoka, M.; Tokunaga, F. Ultrafast photoinduced reaction dynamics of

photoactive yellow protein (PYP): observation of coherent oscillations in the femtosecond fluorescence decay dynamics. *Chem. Phys. Lett.* **2002**, *352*, 220–225.

(8) Chosrowjan, H.; Mataga, N.; Shibata, Y.; Imamoto, Y.; Tokunaga, F. Environmental effects on the femtosecond-picosecond fluorescence dynamics of photoactive yellow protein: chromophores in aqueous solutions and in protein nanospaces modified by site-directed mutagenesis. *J. Phys. Chem. B* **1998**, *102*, 7695–7698.

(9) van Wilderen, L. J. G. W.; van der Horst, M. A.; van Stokkum, I. H. M.; Hellingwerf, K. J.; van Grondelle, R.; Groot, M. L. Ultrafast infrared spectroscopy reveals a key step for successful entry into the photocycle for photoactive yellow protein. *Proc. Natl. Acad. Sci. U.S.A.* **2006**, *103*, 15050–15055.

(10) Groenhof, G.; Schäfer, L. V.; Boggio-Pasqua, M.; Grubmüller, H.; Robb, M. A. Arginine52 controls the photoisomerization process in photoactive yellow protein. *J. Am. Chem. Soc.* **2008**, *130*, 3250–3251.

(11) Coureux, P. D.; Fan, Z. P.; Stojanoff, V.; Genick, U. K. Picometer-scale conformational heterogeneity separates functional from nonfunctional states of a photoreceptor protein. *Structure* **2008**, *16*, 863–872.

(12) van Brederode, M. E.; Gensch, T.; Hoff, W. D.; Hellingwerf, K. J.; Braslavsky, S. E. Photoinduced volume change and energy storage associated with the early transformations of the photoactive yellow protein from *Ectothiorhodospira halophila*. *Biophys. J.* **1995**, *68*, 1101–1109.

(13) Hoff, W. D.; Devreese, B.; Fokkens, R.; Nugteren-Roodzant, I. M.; van Beeumen, J.; Nibbering, N.; Hellingwerf, K. J. Photoinduced volume change and energy storage associated with the early transformations of the photoactive yellow protein from *Ectothiorhodospira halophila*. *Biochemistry* **1996**, *35*, 1274–1281.

(14) Eswar, N.; Webb, B.; Marti-Renom, M. A.; Madhusudhan, M. S.; Eramian, D.; Shen, M. Y.; Pieper, U.; Sali, A. Comparative protein structure modeling using Modeller. *Curr. Protoc. Bioinformatics*; **2006**; Chapter 5:Unit 5.6.

(15) Groot, M. L.; van Wilderen, L. J.; Larsen, D. S.; van der Horst, M. A.; van Stokkum, I. H. M.; Hellingwerf, K. J.; van Grondelle, R. Initial steps of signal generation in photoactive yellow protein revealed with femtosecond mid-infrared spectroscopy. *Biochemistry* **2003**, *42*, 10054–10059.

(16) Heyne, K.; Mohammed, O. F.; Usman, A.; Dreyer, J.; Nibbering, E. T.; Cusanovich, M. A. Structural evolution of the chromophore in the primary stages of trans/cis isomerization in photoactive yellow protein. *J. Am. Chem. Soc.* **2003**, *127*, 18100–18106.

(17) Ihee, H.; Rajagopal, S.; Srajer, V.; Pahl, R.; Anderson, S.; Schmidt, M.; Schotte, F.; Anfinrud, P. A.; Wulff, M.; Moffat, K. Visualizing reaction pathways in photoactive yellow protein from nanoseconds to seconds. *Proc. Natl. Acad. Sci. U.S.A.* **2005**, *102*, 7145–7150.

(18) Rajagopal, S.; Moffat, K. Crystal structure of a photoactive yellow protein from a sensor histidine kinase: Conformational variability and signal transduction. *Proc. Natl. Acad. Sci. U.S.A.* **2003**, *100*, 1649–1654.

(19) Yamaguchi, S.; Kamikubo, H.; Kurihara, K.; Kuroki, R.; Nii-mura, N.; Shimizu, N.; Yamazaki, Y.; Kataoka, M. Low-barrier hydrogen bond in photoactive yellow protein. *Proc. Natl. Acad. Sci. U.S.A.* **2009**, *106*, 440–444.

(20) van Stokkum, I. H. M.; Larsen, D. S.; van Grondelle, R. Global and target analyses of time-resolved spectra. *Biochim. Biophys. Acta* **2004**, *1657*, 82–104.

(21) Hess, B.; Kutzner, C.; van der Spoel, D.; Lindahl, E. GRO-MACS 4: Algorithms for highly efficient, load-balanced, and scalable molecular simulation. *J. Chem. Theory Comput.* **2008**, *4*, 435–447.

(22) Duan, Y.; Wu, C.; Chowdhury, S.; Lee, M. C.; Xiong, G.; Zhang, W.; Yang, R.; Cieplak, P.; Luo, R.; Lee, T.; Caldwell, J.; Wang, J.; Kollman, P. A point-charge force field for molecular mechanics simulations of proteins based on condensed-phase quantum mechanical calculations. *J. Comput. Chem.* **2003**, *24*, 1999–2012.

(23) Mahoney, M. W.; Jorgensen, W. L. A five-site model for liquid water and the reproduction of the density anomaly by rigid, nonpolarizable potential functions. *J. Chem. Phys.* **2000**, *112*, 8910–8922.

- (24) Eswar, N.; Marti-Renom, M. A.; Webb, B.; Madhusudhan, M. S.; Eramian, D.; Shen, M. Y. *Comparative Protein Structure Modeling With MODELLER*. *Current Protocols in Bioinformatics*; John Wiley & Sons, Inc.: 2006; Suppl. 15, pp 5.6.1–5.6.30.
- (25) Bussi, G.; Donadio, D.; Parrinello, M. Canonical sampling through velocity rescaling. *J. Chem. Phys.* **2007**, *126*, 014101.
- (26) Parrinello, M.; Rahman, A. Polymorphic transitions in single crystals: A new molecular dynamics method. *J. Appl. Phys.* **1981**, *52*, 7182–7190.
- (27) Darden, T.; York, D.; Pedersen, L. An Nlog(N) method for Ewald sums in large systems. *J. Chem. Phys.* **1993**, *98*, 10089–10092.
- (28) Essman, U.; Perera, L.; Berkowitz, M. L.; Darden, T.; Lee, H.; Pedersen, L. G. A smooth particle mesh Ewald method. *J. Chem. Phys.* **1995**, *103*, 8577–8592.
- (29) Hess, B.; Bekker, H.; Berendsen, H. J. C.; Fraaije, J. G. E. M. LINCS: A linear constraint solver for molecular simulations. *J. Comput. Chem.* **1997**, *18*, 1463–1472.
- (30) Miyamoto, S.; Kollman, P. A. SETTLE An analytical version of the SHAKE and RATTLE algorithms for rigid water models. *J. Comput. Chem.* **1992**, *13*, 952–962.
- (31) van Aalten, D. M. F.; Haker, A.; Hendriks, J.; Hellingwerf, K. J.; Joshua-Tor, L.; Crielard, W. Engineering photocycle dynamics - crystal structures and kinetics of three photoactive yellow protein hinge-binding mutants. *J. Biol. Chem.* **2002**, *277*, 6463–6468.
- (32) Kort, R.; Hoff, W. D.; Van West, M.; Kroon, A. R.; Hoffer, S. M.; Vlieg, K. H.; Crielard, W.; van Beeumen, J. J.; Hellingwerf, K. J. The xanthopsins: A new family of eubacterial blue-light photoreceptors. *EMBO J.* **1996**, *15*, 3209–3218.
- (33) Larsen, D. S.; van Stokkum, I. H. M.; Vengris, M.; van der Horst, M. A.; de Weerd, F. L.; Hellingwerf, K. J.; van Grondelle, R. Incoherent Manipulation of the Photoactive Yellow Protein Photocycle with Dispersed Pump Dump-Probe Spectroscopy. *Biophys. J.* **2004**, *87*, 1858–1872.
- (34) Baltuska, A.; van Stokkum, I. H. M.; Kroon, A.; Monshouwer, R.; Hellingwerf, K. J.; van Grondelle, R. The primary events in the photoactivation of yellow protein. *Chem. Phys. Lett.* **1997**, *270*, 263–266.
- (35) Devanathan, S.; Pacheko, A.; Ujj, L.; Cusanovich, M.; Tollin, G.; Lin, S.; Woodbury, N. Femtosecond spectroscopic observations of initial intermediates in the photocycle of the photoactive yellow protein from *Ectothiorhodospira halophila*. *Biophys. J.* **1999**, *77*, 1017–1023.
- (36) Ujj, L.; Devanathan, S.; Meyer, T. E.; Cusanovich, M. A.; Tollin, G.; Atkinson, G. H. New photocycle intermediates in the photoactive yellow protein from *ectothiorhodospira halophila*: picosecond transient absorption spectroscopy. *Biophys. J.* **1998**, *75*, 406–412.
- (37) Rupenyan, A.; van Stokkum, I. H. M.; Arents, J. C.; van Grondelle, R.; Hellingwerf, K.; Groot, M. L. Characterization of the primary photochemistry of proteorhodopsin with femtosecond spectroscopy. *Biophys. J.* **2008**, *94*, 4020–4030.
- (38) Changuenet-Barret, P.; Plaza, P.; Martin, M. M.; Chosrowjan, H.; Taniguchi, S.; Mataga, N.; Imamoto, Y.; Kataoka, M. Structural effects on the ultrafast photoisomerization of Photoactive Yellow Protein. Transient absorption spectroscopy of two point mutants. *J. Phys. Chem. C* **2009**, *113*, 11605–11613.
- (39) Mataga, N.; Chosrowjan, H.; Taniguchi, S. Investigations into the dynamics and mechanisms of ultrafast photoinduced reactions taking place in photoresponsive protein nanospaces (PNS). *J. Photochem. Photobiol., C* **2004**, *5*, 155–168.
- (40) Nakamura, R.; Hamada, N.; Ichida, H.; Tokunaga, F.; Kanematsu, Y. Coherent oscillations in ultrafast fluorescence of photoactive yellow protein. *J. Chem. Phys.* **2007**, *127*, 215102–215108.
- (41) Lee, B. C.; Hoff, W. Proline 54 trans-cis isomerization is responsible for the kinetic partitioning at the last-step photocycle of photoactive yellow protein. *Protein Sci.* **2008**, *17*, 2101–2110.
- (42) Takeshita, K.; Imamoto, Y.; Kataoka, M.; Mihara, K.; Tokunaga, F.; Terazima, M. Structural change of site-directed mutants of PYP: new dynamics during pR state. *Biophys. J.* **2002**, *83*, 1567–1577.
- (43) Kyndt, J. A.; Savvides, S. N.; Memmi, S.; Koh, M.; Fitch, J. C.; Meyer, T. E.; Heyn, M. P.; Van Beeumen, J. J.; Cusanovich, M. A. Structural role of tyrosine 98 in Photoactive Yellow Protein: Effects on fluorescence, gateway, and photocycle recovery. *Biochemistry* **2007**, *46*, 95–105.
- (44) Hsiao, Y.-W.; Thiel, W. pB2 Intermediate of the Photoactive Yellow Protein: Structure and Excitation Energies. *J. Phys. Chem. B* **2011**, *115*, 2097–2106.
- (45) Coto, P. B.; Martí, S.; Oliva, M.; Olivucci, M.; Merchán, M.; Andrés, J. Origin of the Absorption Maxima of the Photoactive Yellow Protein Resolved via Ab Initio Multiconfigurational Methods. *J. Phys. Chem. B* **2008**, *112*, 7153–7156.
- (46) Brudler, R.; Rammelsberg, R.; Woo, T. T.; Getzoff, E. D.; Gerwert, K. Structure of the I1 early intermediate of photoactive yellow protein by FTIR spectroscopy. *Struct. Mol. Biol.* **2001**, *8*, 265–270.
- (47) Groenhof, G.; Bouxin-Cademartory, M.; Hess, B.; de Visser, S. P.; Berendsen, H. J. C.; Olivucci, M.; Mark, A. E.; Robb, M. A. Photoactivation of the Photoactive Yellow Protein: Why photon absorption triggers a trans-to-cis isomerization of the chromophore in the protein. *J. Am. Chem. Soc.* **2004**, *126*, 4228–4233.
- (48) Xie, A.; Hoff, W. D.; Kroon, A. R.; Hellingwerf, K. J. Formation of a new buried charge drives a large-amplitude protein quake in photoreceptor activation. *Biochemistry* **1996**, *35*, 14671–14678.
- (49) Kamiya, M.; Saito, S.; Ohmine, I. Proton Transfer and Associated Molecular Rearrangements in the Photocycle of Photoactive Yellow Protein: Role of Water Molecular Migration on the Proton Transfer Reaction. *J. Phys. Chem. B* **2007**, *111*, 2948–2956.
- (50) Boggio-Pasqua, M.; Robb, M. A.; Groenhof, G. Hydrogen bonding controls excited-state decay of the Photoactive Yellow Protein chromophore. *J. Am. Chem. Soc.* **2009**, *131*, 13580–13581.